RESEARCH ARTICLE

SmartMat WILEY

Artificial intelligence-assisted point-of-care testing system for ultrafast and quantitative detection of drug-resistant bacteria

Yang Ding[1,2] | Jingjie Chen[2] | Qiong Wu[1] | Bin Fang[2] | Wenhui Ji[1] |
Xin Li[2] | Changmin Yu[1] | Xuchun Wang[3] | Xiamin Cheng[4] |
Hai-Dong Yu[2] | Zhangjun Hu[5] | Kajsa Uvdal[5] | Peng Li[2] | Lin Li[1,2,6] ● |
Wei Huang[1,2,6]

[1]Key Laboratory of Flexible Electronics (KLOFE) & Institute of Advanced Materials (IAM), Nanjing Tech University (NanjingTech), Nanjing, China

[2]Frontiers Science Center for Flexible Electronics, Xi'an Institute of Flexible Electronics (IFE) and Xi'an Institute of Biomedical Materials & Engineering, Northwestern Polytechnical University, Xi'an, China

[3]College of Chemistry and Material Engineering University of Science and Technology of Anhui, Bengbu, China

[4]Institute of Advanced Synthesis, School of Chemistry and Molecular Engineering, Nanjing Tech University (NanjingTech), Nanjing, China

[5]Department of Physics, Chemistry and Biology, Linköping University, Linköping, Sweden

[6]The Institute of Flexible Electronics (IFE, Future Technologies), Xiamen University, Xiamen, Fujian, China

Correspondence
Lin Li, Peng Li and Wei Huang, Key Laboraroty of Flexible Electronics (KLOFE) & Institute of Advanced Materials (IAM), Nanjing Tech University (Nanjing Tech), Nanjing, China; Frontiers Science Center for Flexible Electronics, Xi'an Institute of Flexible Electronics (IFE) and Xi'an Institute of Biomedical Materials & Engineering, Northwestern Polytechnical University, Xi'an 710072, China.
Email: iamlli@njtech.edu.cn, iampli@nwpu.edu.cn, and vc@nwpu.edu.cn

Abstract

As one of the major causes of antimicrobial resistance, β-lactamase develops rapidly among bacteria. Detection of β-lactamase in an efficient and low-cost point-of-care testing (POCT) way is urgently needed. However, due to the volatile environmental factors, the quantitative measurement of current POCT is often inaccurate. Herein, we demonstrate an artificial intelligence (AI)-assisted mobile health system that consists of a paper-based β-lactamase fluorogenic probe analytical device and a smartphone-based AI cloud. An ultrafast broad-spectrum fluorogenic probe (**B1**) that could respond to β-lactamase within 20 s was first synthesized, and the detection limit was determined to be 0.13 nmol/L. Meanwhile, a three-dimensional microfluidic paper-based analytical device was fabricated for integration of B1. Also, a smartphone-based AI cloud was developed to correct errors automatically and output results intelligently. This smart system could calibrate the temperature and pH in the β-lactamase level detection in complex samples and mice infected with various bacteria, which shows the problem-solving ability in interdisciplinary research, and demonstrates potential clinical benefits.

Yang Ding, Jingjie Chen, and Qiong Wu contributed equally to this study.

---

1 | INTRODUCTION

The discovery and development of antibiotics undoubtedly represent milestone achievements in the defense against pathogenic bacteria, and millions of lives have been saved.[1] However, fast-emerging antimicrobial resistance (AMR) is an inevitable consequence of the overuse and misuse of antibiotics and has become a global healthcare crisis.[2,3] The expression of β-lactamase is the main factor responsible for the resistance toward β-lactams, which is a widely used class of antibiotics.[4,5] Methicillin-resistant *Staphylococcus aureus* (MRSA), the most common gram-positive bacterial pathogen that can express β-lactamase, has spread globally, and become the leading cause of pathogenic infections in both community settings and global healthcare.[6] Besides, gram-negative bacteria, including *Escherichia coli* (*E. coli*), *Klebsiella pneumoniae* (*K. pneumoniae*), and *Enterobacter cloacae* (*E. cloacae*), can also develop severe resistance to β-lactam antibiotics due to their gradual generation of β-lactamase, and nowadays, their various subtypes have spread all over the world.[7,8] In view of the possibility that the global situation of AMR could become more serious, the detection and identification of drug-resistant bacteria are particularly important.[9–13]

Over the past few decades, the detection methods of β-lactamase primarily relied on phenotypic, genic, and enzymatic assays.[14–16] However, these conventional methods are usually not time efficient. Although polymerase chain reaction and mass spectrometry have yielded outstanding results,[17] these methods typically have high costs and are time/labor-consuming, limiting their applications in point-of-care testing (POCT). Fortunately, a fluorogenic probe can be used as a powerful tool for POCT due to its high sensitivity, efficiency, and low cost.[18] In recent years, some β-lactamase fluorogenic probes have been developed (Supporting Information: Figure S1) and applied in POCT.[19–23] Rao et al. developed *Mycobacterium*

tuberculosis-specificity fluorogenic probes (CDG-OMe and CDG-DNB3) and applied them in a microfluidic chip, showing the POCT ability of tuberculosis.[9,10] Jiang et al. reported a broad-spectrum fluorogenic probe (CDG-1) that allows for the POCT of β-lactamase in milk samples.[21] Notwithstanding, specific fluorogenic probes capable of rapidly reacting with β-lactamase remain to be elucidated. This deficiency often leads to missed optimal treatment due to the inability to quickly identify infection with drug-resistant bacteria in some emergency rescues. Therefore, a fluorogenic probe with ultrafast reaction ability with β-lactamase is very important.

With the incorporation of POCT, a disposable, capable of quantitative and intellective analysis, and inexpensive analytical device for diagnosis of AMR that does not require instrumentation or trained laboratory personnel for analysis is highly needed. A microfluidic paper-based analytical device (μPAD) is a low-cost and easy-to-operate tool with instant testing capacity that has shown significant promise as an alternative platform for diagnostics in POCT.[24,25] Henry et al. directly applied μPAD in AMR bacteria detection, demonstrating the presence of β-lactamase-mediated AMR bacteria in sewage.[26] These devices dispense with the procedures of transporting samples to central laboratories for slow and labor-intensive testing that is usually required when monitoring AMR bacteria. However, the unstable factors of temperature, pH, and other environmental variables in the practical experiments can affect the test results, thereby causing errors or even misdiagnosis, especially for the diagnosis mechanisms that are based on enzymatic reactions. Hence, the auxiliary function of smart devices and the data processing ability of cloud computing to automatically correct test errors in the POCT play a vital role in practical applications. Fortunately, a mobile health (mHealth) system integrating microfluidic-based biosensors and smart devices enables the measurement of biochemical markers.[27,28] Due to the advantages of data processing, digital output, and user-friendliness,

the landscape of mHealth is rapidly expanding. Meanwhile, smartphones, as an attractive terminal for the mHealth system due to their widespread use, inbuilt features, and ubiquity, have allowed the mHealth system to aid in the disease management of patients in POCT settings, digitally bridging patients and healthcare professionals.[29,30]

Herein, to enable rapid determination of drug-resistant bacteria and automatic test error correction in complex environments, we proposed an artificial intelligence (AI)-assisted mHealth system for the detection of drug-resistant bacteria in POCT, where three-dimensional (3D) microfluidic paper-based β-lactamase fluorogenic analytical devices and a smartphone-based AI cloud were rationally combined. Due to inter-disciplinary efforts, this system consists of the following three units: (1) a newly designed fluorogenic probe that can rapidly respond to β-lactamase; (2) microfluidic sensors with complex and delicate 3D μPAD capacity that can be applied to load the β-lactamase fluorogenic probe; and (3) generated based on AI technology, a smartphone-based AI cloud that can automatically process data, intelligently correct errors, and digitally output results of 3D μPAD's images taken by a smartphone.

2 | EXPERIMENTAL SECTION

2.1 | Materials and instruments

All proteins and analytes including β-lactamase (TEM-1), various enzymes, and amino acids were purchased from Sigma-Aldrich. All the chemical reagents were purchased from Aldrich or TCI. Commercially available reagents were used without further purification. Anhydrous solvents for organic synthesis were distilled over CaH_2. Reaction progress was monitored by TLC on precoated silica plates (250 μmol/L thickness) and spots were visualized by UV light or iodine. ^{1}H- and ^{13}C-NMR spectra were measured using a JOLE-400 MHz. Coupling constants (J value) are reported in Hertz. Mass spectrometry was carried out using Autoflex speed MALDI-TOF. Absorption spectra were recorded using the Synergy HTX Microplate Reader or a Shimadzu UV-1750 spectrophotometer. Photoluminescent spectra were recorded using the BioTek Cytatio5 Cell Imaging Multi-Mode Reader or an F-7000 fluorescence spectrophotometer. The 3D μPAD was fabricated using a Whatman® quantitative filter paper, ashless, Grade 4 (GE Healthcare Life Science), 5 × 5 cm, using a simple design of patterns with Microsoft Office 2016 and printed through a FUJI XEROX Phaser 8560DN wax printer. The

images of the 3D μPAD were recorded using an iPhone X's Camera. The fluorescence spectra of the 3D μPAD were measured using a Digital Colorimeter (App. that comes with Mac OS X). The temperature of the test environment was regulated using the DHG-9070A electric blast drying oven or the THZ-100 constant temperature shaker. *E. coli* (American Type Culture Collection [ATCC] 25922), *S. aureus* (ATCC 29213), Multidrug-resistant *E. cloacae* (ATCC 13047), and *K. pneumoniae* (ATCC 13883) were obtained from the ATCC. Multidrug-resistant *S. aureus* strains of MRSA ZJU and MRSA USA 300 were isolated from Zhejiang University and Peking University Third Hospital (PKU). Multidrug-resistant *K. pneumoniae* strains were isolated from PKU and the Xi'an Jiaotong University Health Science Center (XJTU). The β-Lactamase activity commercial kit (nitrocefin, CAS number: 41906-86-9) was obtained from Delta Biotechnology Co., Ltd. The smartphone-based AI cloud was written in Python 3.0 and Open CV for Macintosh and run using the terminal of a Mac OS X system.

2.2 | Preparation of TEM-1 stock solutions

The stock solution of the probes was prepared in dimethyl sulfoxide (DMSO) at a concentration of 1 mmol/L and restored in a −20°C refrigerator for further usage. For the test of spectroscopic properties, a volume of 10 μL of 10 μmol/L TEM-1 stock solution was injected into 1 mL of deionized water to yield a detection solution with a probe concentration of 10 μmol/L. After the addition of the analytes, the mixture was shaken for 5 min, and then measured using a microplate reader.

2.3 | Limit of detection

The calibration curve was obtained from the plot of the fluorescence intensity at 530 nm as a function of the TEM-1 concentration. The detection limit $= 3 \times \sigma/K$, where K is the slope of the curve equation and σ represents the standard deviation of the fluorescence intensity of B1 in the absence of TEM-1 at 530 nm in phosphate-buffered saline (PBS) buffer.

2.4 | Enzymatic kinetics

Different concentrations of the A1/B1 (10, 20, 40, 60, 80, 100 μmol/L) in PBS (10 mmol/L, pH 7.4, containing 2% DMSO) in a 384-well plate were added with TEM-1. The

fluorescence intensity at 530 nm was measured in a microplate reader at room temperature. The values of the kinetic parameters (K_m and k_{cat}) were determined from the standard Lineweaver–Burk plot.[31]

2.5 | Docking study of probes with TEM-1

Protein preparation: The TEM-1 crystal structure (PDB: 5HVI) used for docking was downloaded from the protein databank. The protein was generated by removing water molecules and other bound ligand molecules using Discovery Studio 2016. The binding site of protein was defined after adding polar hydrogens to TEM-1 using a grid box from AutoDockTools from MGL 1.5.6 (The Scripps Research Institute). Ligand preparation: Ligand was prepared by AutoDockTools from MGL 1.5.6 (The Scripps Research Institute) for docking by AutoDock Vina. Docking: Docking was performed using AutoDock Vina and visualized using Pymol viewer.[32]

2.6 | Fabrication of 3D µPAD

The 3D paper was filter paper (Whatman® quantitative filter paper, 5×5 cm) patterned by a wax printer. The filter paper was then heated on a hotplate to melt the wax area at a temperature of 100°C.[33] The white area was the hydrophilic wax area. Then, 15 µL of fluorescein derivative (50 µmol/L) and 15 µL of B1 (50 µmol/L) solution were dropped into holes 2 and 3 of the detecting pad area, respectively, which was dried in a fume hood for 20 min.

2.7 | Procedure for testing TEM-1 by 3D µPAD

TEM-1 in PBS (20 µL, 10 mmol/L, pH 5.8–8.2) in different concentrations was directly dropped onto the sampling pad at different temperatures (4–48°C). After 15–20 min, the image of the fluorescence signal of the detecting pad was recorded using an iPhone X and the RGB value was calculated using a digital colorimeter.

2.8 | Stability of 3D µPAD

The 3D A1-µPAD and 3D B1-µPAD were placed in a sealed bag with oxygen removed, and then the sealed bag was placed in a 4°C refrigerator and a room-temperature environment for 1 week. It was taken out at a fixed time

point every day and the level of self-decomposition of 3D µPAD was calculated. The self-decomposition efficiency of 3D PAD can be obtained by plotting ln $[(S_0/S_0 - P)]$ with time (h) and calculating the slope. S_0 is the initial concentration of fluorogenic probes in hole 3 in 3D PAD and P is the concentration of the fluorescein derivative generated by decomposition.

2.9 | Bacteria activation and resistance assays

To evaluate the resistance of different strains to β-lactam antibiotics, the MIC of cephalothin (an advanced β-lactam) against 10 strains was determined according to the reported protocol,[34] which are *E. cloacae* (ATCC 13047), *K. pneumoniae* (ATCC 13883, two drug-resistant clinical isolates), *E. coli* (ATCC 25922, a drug-resistant clinical isolate), and *S. aureus* (ATCC 29213, MRSA USA300, and a drug-resistant clinical isolate). Briefly, the selected colonies were inoculated and cultured in Mueller–Hinton Broth (MHB) medium until the mid-log growth phase. The bacterial suspensions were diluted with fresh MHB to a concentration of ~10^5 colony-forming units per milliliter (CFU/mL). 50 µL of $2 \times$ MHB and cephalothin were added to the first column of the 96-well plate, and 50 µL of MHB was added to the remaining 11 columns. Cephalothin was diluted in half from the first column to the tenth column and 50 µL of antibiotics and bacterial suspensions were added to the 11th column and the 12th column, respectively, as a negative and a positive control group. The plates were incubated at 37°C for 16 h. Afterwards, the value of MIC was determined from the wells with no visible bacterial growth. In addition, the mid-log growth phase microorganisms were collected by centrifugation (at 1000g for 5 min) and resuspended in sterile PBS to adjust the concentration to ~10^8 CFU/mL. Next, different concentrations (~10^7, 10^6, and 10^5 CFU/mL) of bacterial suspensions were obtained by 10-, 100-, and 1000-fold dilutions of the sample, respectively, and stored in refrigerators for later use.

2.10 | Working mechanism of the mHealth system

After ultrasonic lysis of different concentrations of bacteria suspensions, the liquid (20 µL) was directly dropped on the 3D B1-µPAD at room temperature. After 20 min, the fluorescence photos were taken using a smartphone in a confined space. The excitation sources were handheld UV lamps (365 nm) with 6 W. The images

of 3D B1-µPAD were uploaded and analyzed by the smartphone-based AI cloud.

2.11 | Animal studies

Four groups of 12 Kunming mice (6–8 weeks old, male) were used for the peritonitis model, and the other four groups were used for the full-thickness skin wound infection model. For the peritonitis model, the mice were intraperitoneally injected with 100 µL of saline containing ~10^5 CFU/mL and ~10^7 CFU/mL of *E. coli* (ATCC 25922 and drug-resistant clinical isolate), respectively. At 3, 6, 12, and 24 h after bacteria inoculation, the ascites were collected for mHealth system detection and were also placed on LB agar plates for colony counting. At the same time, a commercial kit (nitrocefin; β-lactamase activity kit) was used to confirm the accuracy of the mHealth system. At 24 h after injection, the mice were administered anesthesia, and then their hearts, spleens, lungs, and kidneys were collected for observation. For the mice full-thickness skin wound infection model, the dorsal region of each mouse was shaved and depilated after anesthetization, and then cleaned with 75% ethanol. Two full-thickness wounds (6 mm in diameter) were created on the upper back of each mouse by dermal biopsy punches. The wounds were inoculated with exactly 20 µL of *S. aureus* and MRSA ZJU suspension (~10^5 CFU/mL and 10^7 CFU/mL, respectively).[35] All wounds were covered with a 3M Micropore™ tape, and mice were individually housed. The wounds were observed every 12 h and wound exudate was collected for testing.

3 | RESULTS AND DISCUSSION

3.1 | General strategy of the mHealth system

In this mHealth system, the central detecting unit was the designed and synthesized fluorogenic probes with an ultrafast response to β-lactamase. A general strategy involved taking advantage of the characteristic that β-lactamase can hydrolyze the β-lactam quaternary ring, and the detection was performed by determining the changes in the fluorescence intensity after the reporter on probes was released. In this unit, we designed two broad-spectrum fluorogenic probes (A1/B1) using cephalothin as the recognizer of β-lactamase (Figure 1A). As the first-generation cephalosporin, cephalothin can be hydrolyzed by all types of β-lactamases, which determines the broad-spectrum property of A1/B1.

Meanwhile, fluorescein derivative as a reporter has the advantage of high fluorescent brightness. This design was intended to ensure the excellent spectral performance of probes together with high selectivity and sensitivity toward β-lactamase. To improve the sensitivity of the probes and their reaction rates with β-lactamase, we chose the carbonate unit as the reactive linker between the cephalothin and the fluorescent reporter in B1. We envisioned that the carbonate might respond fast to the β-lactamase-catalytic cleavage reaction, therefore allowing the rapid release of the fluorescent reporter.[36,37] The chemical synthesis of A1/B1 is described in the Supporting Information in detail. All these compounds were successfully characterized by ^{1}H-NMR, ^{13}C-NMR, and HRMS spectra as shown in Supporting Information: Figures S12–S31.

The fabrication of 3D µPAD (Figure 1B) involved the use of a Whatman® filter paper as the base, the editing of personalized patterns on a computer, and printing with a wax printer to form hydrophilic–hydrophobic barriers. Three layers were integrated to develop a low-cost, green, flexible, and convenient analysis device that could be used for sampling, shunting, and detecting, all of which could be accomplished within one device.

The data processing and output unit were performed on the smartphone-based AI cloud (Figure 1C). The overall implementation was accomplished due to the ability of the smartphone-based AI cloud to intelligently analyze the information on the 3D fluorogenic probe-µPAD images that were shot and uploaded by the smartphone. At the back end of the smartphone-based AI cloud, computer vision technology was applied for the perception and recognition of personalized patterns on the 3D fluorogenic probe-µPAD. Meanwhile, a database for cloud computing achieved based on the fitting curves of an enzyme reacted with the 3D fluorogenic probe-µPAD at different temperatures and under different pH conditions was established to calculate and automatically correct test errors. Then, the result in the form of digital output was visualized at the front end of the smartphone.

3.2 | Photophysical properties of probes A1 and B1

First, we investigated the spectral properties of A1 and B1 toward TEM-1 (the most common type of β-lactamase). A1 and B1 initially showed the main UV–*vis* absorption peak at 380 and 370 nm, respectively, while the maximum absorption peak shifted to 450 nm upon the addition of TEM-1 (Figure 2A,B). The fluorescence of A1 and B1 in solution was negligible due to the fluorescein derivative being locked in the lactonization
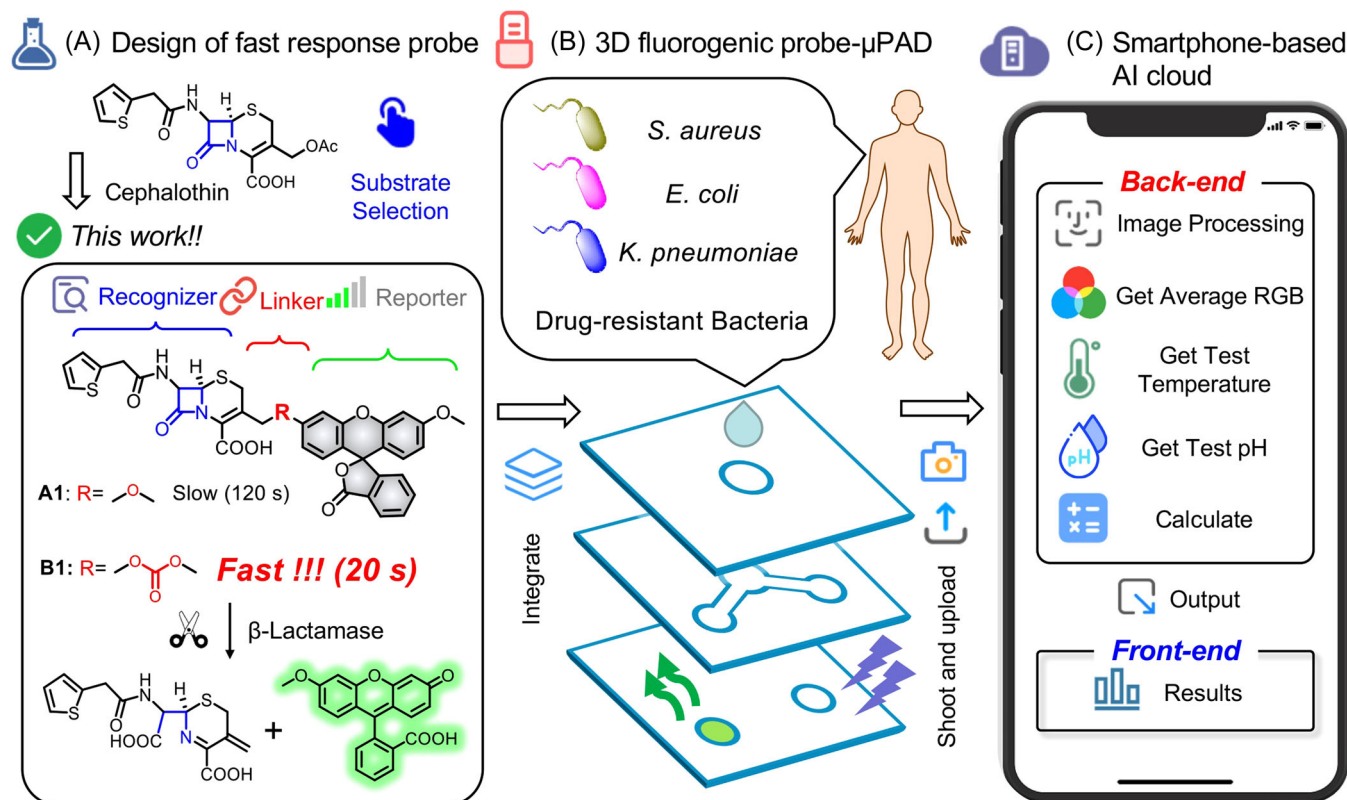
FIGURE 1 General strategy of a fluorogenic probe-based mHealth system. (A) Design strategy of the reaction-based β-lactamase fluorogenic probe A1/B1. After the A1/B1-specific recognizer cephalothin's β-lactam ring was opened by β-lactamase, the linkers were broken to release the reporter. (B) Model of the three-dimensional (3D) probe-microfluidic paper-based analytical device (μPAD). Three layers of sampling, shunting, and detecting pad were manually assembled to form the integrated 3D B1-μPAD. (C) Overall implementation for a smartphone-based artificial intelligence (AI) cloud. The procedure and each program modules were developed together to generate the result at the back-end of a smartphone-based AI cloud, and the result was then transferred to the front–end of the smartphone.

format of probes. Upon the addition of TEM-1, the β-lactam quaternary ring was hydrolyzed to generate a free fluorescein derivative, which yielded significant fluorescent signal enhancement at around 530 nm (Figure 2C). Meanwhile, as the concentration of TEM-1 was increased, the fluorescence intensity of A1/B1 increased in a curve-shaped manner (Figure 2D). In addition, kinetics experiments of A1 and B1 with TEM-1 were performed by time-dependent fluorescence analysis. It was noted that the fluorescence intensity of B1 increased sharply and reached a plateau after ~20 s of TEM-1 (100 nmol/L) addition, which is much faster than that of A1 (>2 min) (Figure 2E). This observation fully confirms our hypothesis that the active carbonate bond can obviously accelerate the cleavage rate of the linker. Then, the values of the apparent Michaelis–Menten constant K_m and the catalytic constant k_{cat} of B1 in response to TEM-1 were calculated to be 14 μmol/L and 76 s^{-1}, respectively. The catalytic efficiency K_{app} (k_{cat}/K_m) was calculated to be 5.4×10^6 L/(mol·s), which is higher

than that of most β-lactamase fluorogenic probes that have been reported (Supporting Information: Table S1).

To further confirm our hypothesis, a molecular docking simulation was performed to identify the binding mode of A1/B1 with TEM-1 (Figure 2F,G). Due to presence of the same recognizer and reporter in A1/B1, the simulation data of the docking affinity (−7.8/−7.5 kcal/mol) indicate that A1/B1 interacts stably with the protein. The distances between the substrate of A1/B1 and some of the important active residues such as Ser70, Val237, Lys234, and Ser130 are very close,[38] which indicates that the hydrolysis efficiency of A1/B1 is catalyzed by TEM-1 as a relatively horizontal line (Figure 2H). However, B1 can obtain a fluorescence signal faster than A1 after reacting with TEM-1, which confirms our hypothesis that once the selection of a target and a specific substrate is fixed, the release efficiency of the reporter can be improved by upregulating the activity of the linker. Therefore, we chose B1 for further determination of β-lactamase.
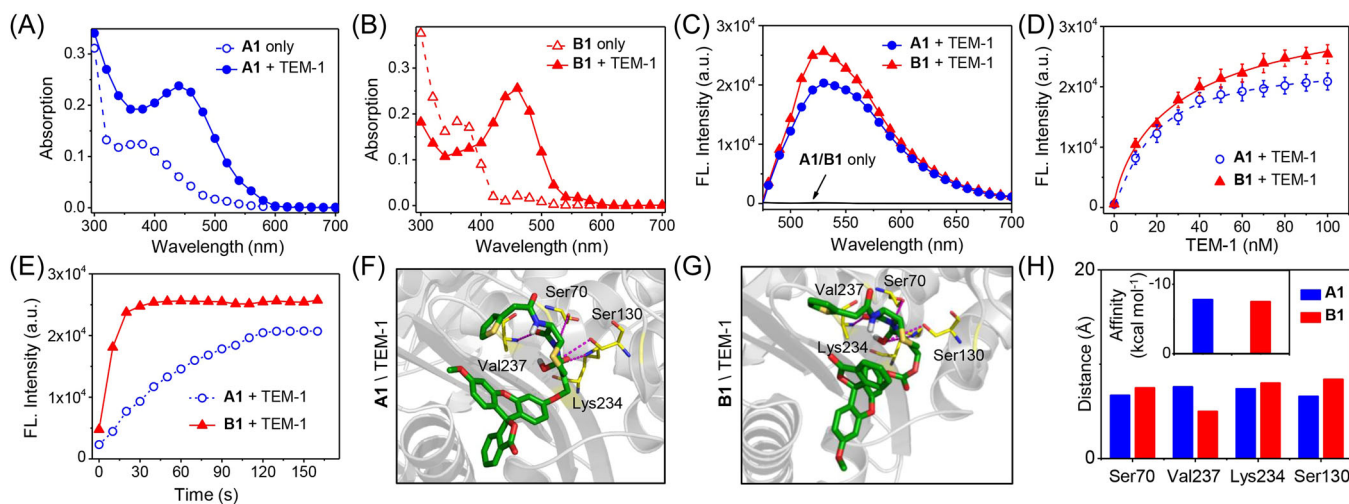
FIGURE 2 Photophysical and docking properties of A1/B1. (A) Absorption spectra of A1 and (B) B1 (10 μmol/L) reacting with TEM-1 in phosphate-buffered saline (PBS) buffer (10 mmol/L, pH 7.4, containing 2% DMSO) at room temperature. (C) Emission spectra of A1/B1 (10 μmol/L) reacting with TEM-1 (100 nmol/L) in PBS buffer (10 mmol/L, pH 7.4, containing 2% DMSO) at room temperature. (D) Linear relationship of fluorescence intensities at 530 nm of A1/B1 (10 μmol/L) reacting to different concentrations TEM-1 (0–100 nmol/L) in PBS buffer (10 mmol/L, pH 7.4, containing 2% DMSO) at room temperature ($n = 3$ independent experiments). (E) Time-dependent fluorescence intensities at 530 nm of A1/B1 (10 μmol/L) reacting with TEM-1 (100 nmol/L) in PBS buffer (10 mmol/L, pH 7.4, containing 2% DMSO) at room temperature. (F) Molecular docking of probes A1 and (G) B1 in the binding pocket of TEM-1 (PDB ID: 5HVI). (H) Distance and docking affinity (inset) of A1/B1 in the binding pocket of TEM-1.

Under the above-determined conditions, the detection ability of B1 at a low concentration of β-lactamase was tested (Supporting Information: Figure S4A). The fluorescence response of B1 to TEM-1 shows good linearity in the concentration range of 0–10 nmol/L (Supporting Information: Figure S4B). In addition, the detection limit with respect to TEM-1 was determined to be 0.13 nmol/L. Meanwhile, to study the specificity of the B1 toward β-lactamase, we measured the fluorescence response of B1 to 100 nmol/L of TEM-1 and other substances including various enzymes (such as TYR, NTR, GGT, BSA, MAO A, MAO B), ions, amino acids, and other biomolecules in parallel at room temperature in 20 s (Supporting Information: Figure S5). Only TEM-1 caused obvious fluorescence enhancement, while the others induced negligible fluorescence changes. Therefore, it is apparent that B1 has outstanding specificity toward TEM-1 in complex biological environments. Furthermore, to demonstrate the broad-spectrum performance, we tested the ability of B1 to react with AmpC (a type of class C β-lactamase) and CTX-M-14 (a type of extended-spectrum β-lactamase). The result shows that B1 is a broad-spectrum probe for detecting various β-lactamase (Supporting Information: Figure S6). The above performances of B1, including excellent selectivity, fast response, low detection limit, broad spectrum toward β-lactamase, and so on, confirmed the rationale of our molecular design concept and lay the foundation for the fabrication of 3D μPAD for use in the detection of drug-resistant bacteria under POCT conditions.

3.3 | Design and fabrication of 3D μPAD

Translating the concept at the laboratory level into products that users can afford is an important step in the POCT area. After demonstrating the probe structure design concept, we integrated the 3D μPAD with B1 to develop a POCT device with the capacity for β-lactamase detection. Sampling, shunting, and detecting paper pads were assembled using transparent glue to form the integrated 3D B1-μPAD, which were composed of the hydrophilic area (white part) and the hydrophobic area (black part) that were printed with wax. The hydrophilic area of the detecting pad consisted of hole 1 (blank, as a baseline control), hole 2 (impregnated with a free fluorescein derivative), and hole 3 (impregnated with B1) (Figure 3A). Figure 3B shows the process of the 3D B1-μPAD detection of β-lactamase.

First, the performances of the spectral response of 3D B1-μPAD with different concentrations of TEM-1 were recorded using a camera-equipped smartphone, and the RGB value was calculated using a Digital Colorimeter (an app that comes with Mac OS X). Due to the presence of β-lactamase, which induced a green-colored emission, the intensity of the green channel (G value in RGB) is the decisive parameter for evaluating β-lactamase levels. It
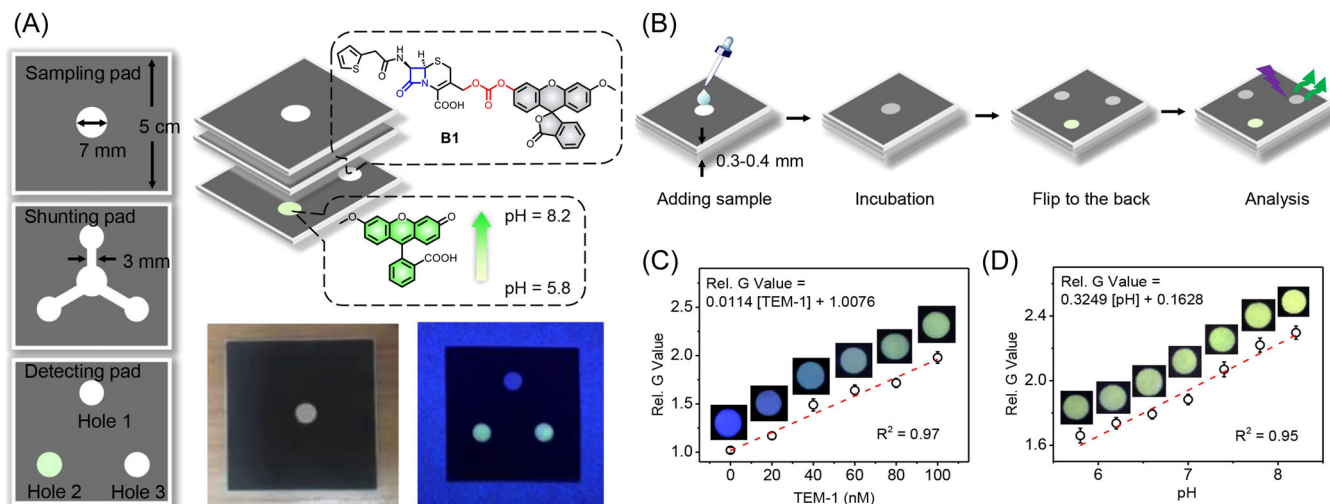
FIGURE 3 Schematic of three-dimensional (3D) B1-μPAD. (A) Representation and photographs of the 3D B1-μPAD. (B) Test procedure of 3D B1-microfluidic paper-based analytical device (μPAD). (C) Linear relationship of Rel. G value of hole 3 of 3D B1-μPAD as a function of TEM-1 (0–100 nmol/L) at room temperature. Inset: Gradual changes in the color of hole 3 of 3D B1-μPAD after adding different concentrations of TEM-1 (0–100 nmol/L) under a UV lamp (ca. 365 nm) ($n = 3$ independent experiments). (D) Linear relationship of Rel. G value of hole 2 of 3D B1-μPAD as a function of pH (5.8–8.2) at room temperature. Inset: Gradual changes in the color of hole 2 of 3D B1-μPAD at different pH (5.8–8.2) and phosphate-buffered saline buffer (10 mmol/L) ($n = 3$ independent experiments).

should be noted that to eliminate the influence of the angle and brightness of the excitation light on the image data of 3D B1-μPAD, we set the G value of hole 1 (control) as "1" and that of holes 2 and 3 as the relative value (Rel. G value = G value$_{\text{hole 2 or 3}}$/G value$_{\text{hole 1}}$). On adding different concentrations of TEM-1, a significant change in the Rel. G value occurred and increased gradually in hole 3, and the Rel. G value showed a good linear relationship at the concentration of TEM-1 ranging from 0 to 100 nmol/L (Figure 3C). It was noted that when the sample entered the 3D B1-μPAD, due to the interaction of the paper and the binding force of cellulose, some enzymes were immobilized on the paper, which affected the progress of the enzymatic reaction. This may explain why the fitting curve of 3D B1-μPAD reacting with TEM-1 was a straight line.[24] Interestingly, the Rel. G value of the dye in hole 2 increased with increasing pH and also showed a good linear relationship (Figure 3D), which may be due to the influence of pH on the disruption of fluorescein derivative lactonization.[39] This means that hole 2 can be used as an indicator of the pH of the sample, thus subsequently facilitating our design of pH calibration in the smartphone-based AI cloud subsequently. Furthermore, we tested the stability of 3D B1-μPAD. The self-decomposition efficiency of 3D **B1**-μPAD is as low as $3.86 \times 10^{-3}\,\text{h}^{-1}$ and $4.54 \times 10^{-3}\,\text{h}^{-1}$ at 4°C and 25°C, respectively, which is almost the same as that of 3D A1-μPAD (Supporting Information: Figure S7). This indicates that 3D B1-μPAD has good stability during its use in POCT.

3.4 | Construction of the smartphone-based AI cloud

Temperature and pH are important parameters that affect POCT. In real practice, the test may be conducted in freezing/hot conditions in the winter/summer and for samples with different values of pH. Here, we tested β-lactamase activity with 3D B1-μPAD and a commercial kit (nitrocefin; β-lactamase activity kit). The results showed high sensitivity to the temperature and pH (Supporting Information: Figure S8). This may lead to the inaccurate quantification of β-lactamase levels and resistant bacteria in POCT. To eliminate the influence of temperature and pH on 3D B1-μPAD and to achieve suitable testing, we established the smartphone-based AI cloud and combined it with 3D B1-μPAD to develop the mHealth system. This method was formulated to use the images of the 3D B1-μPAD shot by a smartphone and upload them to a smartphone-based AI cloud for intelligent data analysis. The overall website framework of the smartphone-based AI cloud was built by Django, and the item directory of Django is shown in Supporting Information: Figure S2. The main menu of the front end includes login, upload, and an index interface (Figure 4A), whereas the back end includes the cloud server, where the images of 3D B1-μPAD are processed and analyzed. The operation mode is as follows: users enter the smartphone-based AI cloud through the login interface at the front end and upload the images to the back end; the back end then digitally transmits the
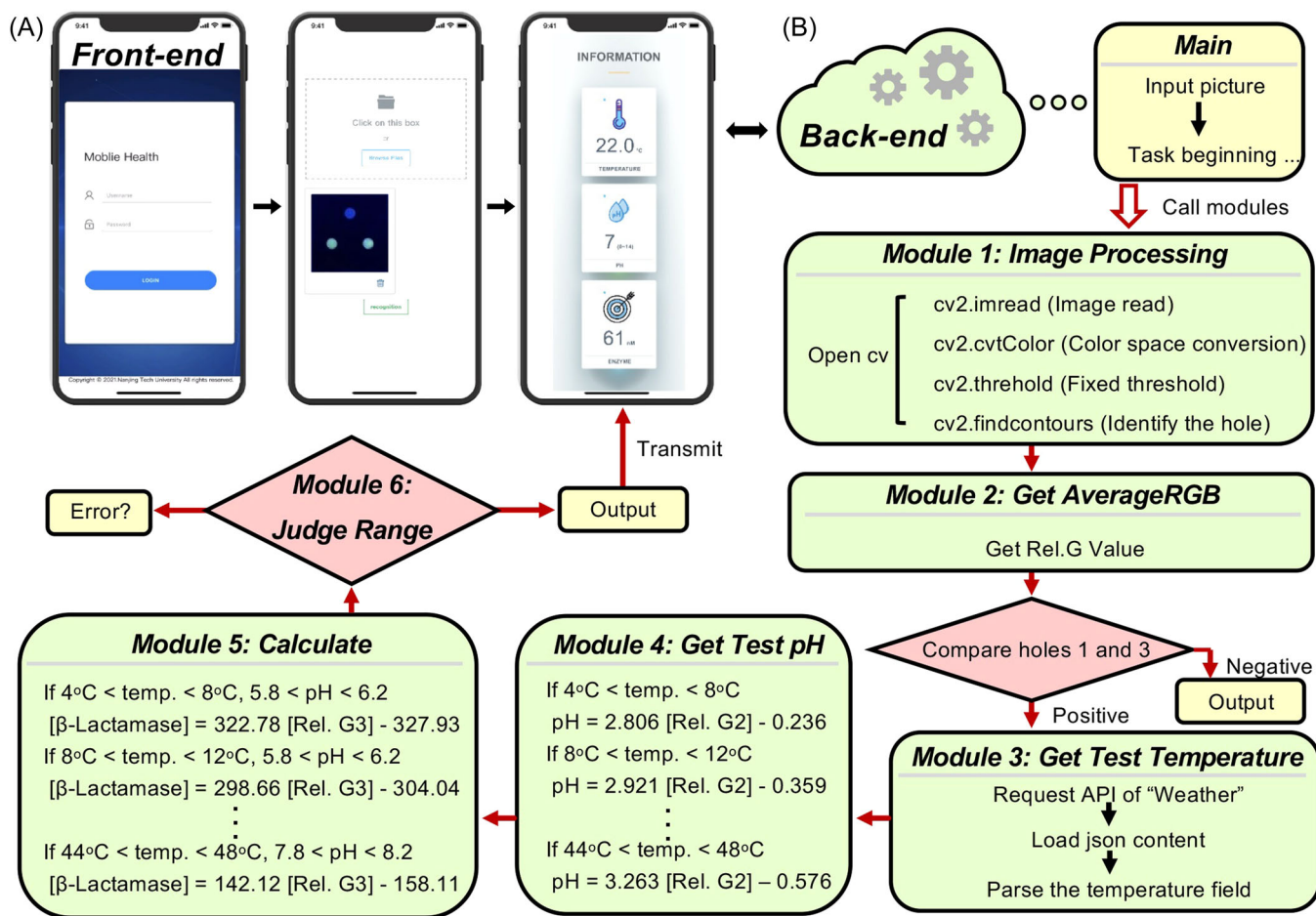
FIGURE 4 Operational process of the smartphone-based artificial intelligence cloud. (A) Main menu and login, upload, and index interface of the front end. (B) Running route of the back end and the function of each module in it.

information of an image to the index interface at the front end. The main technology stacks used in the smartphone-based AI cloud are shown in Supporting Information: Figure S3.

The back end is the core unit of data processing and cloud computing, and takes place on the smartphone-based AI cloud. The code of the back-end frame was mainly divided into six main modules. The running route of the back end involves the main module, which first obtains the image of 3D B1-μPAD and in turn calls for each module to serve its function. *Def 1 ImageProcessing* identifies the round hole (holes 1–3) in the collection image through computer vision. This module reads the uploaded images and converts their colors into spatial values and fixed thresholds, finally finding the round hole. This module was written in Python-Opencv and the imported code was from cv2. *Def 2 GetAverageRGB* converts the color in the hole into the corresponding average RGB value and determines the Rel. G value. If the Rel. G value$_{hole\ 3} < 1.1$, it is considered negative.

Otherwise, the next module will proceed. *Def 3 GetWeather* first requests the application programming interface (API) of "Weather," then loads the JSON content and extracts the temperature value to obtain the real-time test environment temperature (e.g., the city of Nanjing). *Def 4 GetTestpH* calculates the pH through the fitting function of the Rel. G value$_{hole\ 2}$ and pH (5.8–8.2) at different temperatures (4–48°C) (Supporting Information: Table S2) to obtain the pH of the test buffer. *Def 5 Calculate* calculates the β-lactamase level in the database, which is a fitting function of the Rel. G value$_{hole\ 3}$ and the β-lactamase concentration at different temperatures (4–48°C) and pH (5.8–8.2) (Supporting Information: Table S3). *Def 6 JudgeRange* analyzes and processes the data obtained from the calculation and outputs the β-lactamase levels (Figure 4B). Details on the source code of smartphone-based AI cloud are provided in the Supporting Information or freely available online through GitHub at https://github.com/Younger188/Chemistry_django.

3.5 | mHealth system detection of β-lactamase in bacteria

In this mHealth system, only a 3D B1-μPAD, a box, a UV light source, and a smartphone are needed; all these items can be found commonly, allowing users to monitor β-lactamase levels in various states. The 3D B1-μPAD was placed in a box to limit light exposure, and an excitation light was shined into the space. Then, an image of 3D B1-μPAD was captured by a smartphone and then directly uploaded onto the smartphone-based AI cloud, where it was analyzed and provided the corresponding value of β-lactamase level (Figure 5A). All the equipment involved in the mHealth system are accessible and easily accessible, even in remote areas. Supporting Information: Movie S1 shows the whole detection process in detail.

To demonstrate its ability to detect β-lactamase in live bacteria, the mHealth system was applied to test the levels of β-lactamase at different concentrations in normal and drug-resistant bacteria. All the Rel. G values of antibiotic-sensitive groups including *S. aureus*, *E. coli*, and *K. pneumoniae* tested by the mHealth system were around 1.1, whereas those of multidrug-resistant
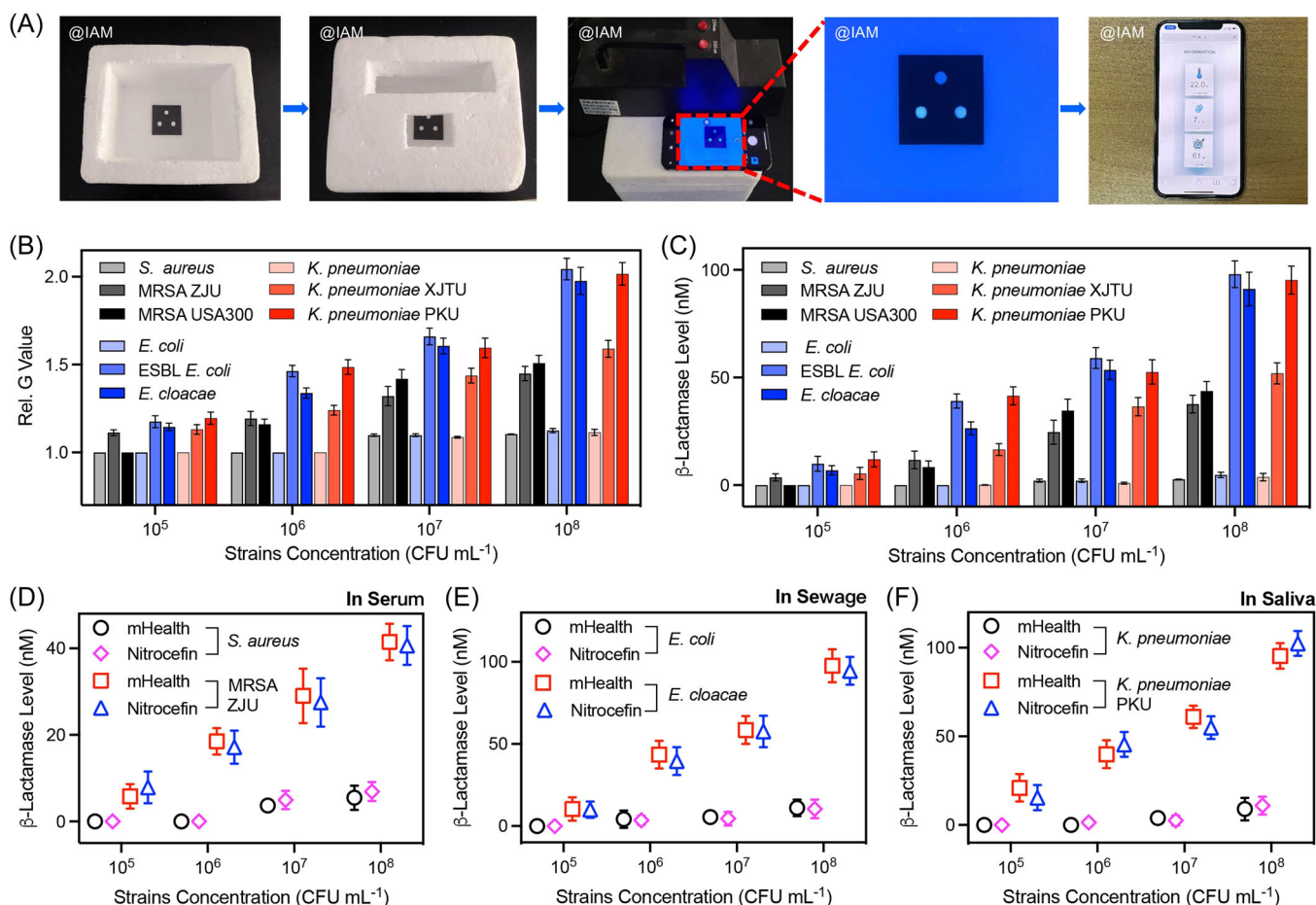

FIGURE 5 Mobile health (mHealth) system detection of β-lactamase levels in bacteria. (A) Working mechanism of the mHealth system. (B) Rel. G value of the mHealth system obtained from the test of antibiotic-sensitive *Staphylococcus aureus* and clinically isolated multidrug-resistant *S. aureus* (MRSA) (MRSA ZJU and MRSA USA300), antibiotic-sensitive *Escherichia coli*, and clinically isolated extended-spectrum β-lactamase (ESBL) *E. coli* and *Enterobacter cloacae*, antibiotic-sensitive *Klebsiella pneumoniae*, and clinically isolated multidrug-resistant *K. pneumoniae* (Xi'an Jiaotong University Health Science Center [XJTU] and Peking University Third Hospital [PKU]) in different concentrations (~10^5, 10^6, 10^7, and 10^8 CFU/mL) in phosphate-buffered saline buffer (10 mmol/L, pH 5.8–8.2) at 25°C and 37°C ($n = 3$ independent experiments). (C) β-Lactamase levels in *S. aureus*, MRSA ZJU, MRSA USA300, *E. coli*, ESBL *E. coli*, *E. cloacae*, *K. pneumoniae*, XJTU, and PKU *K. pneumoniae* at different concentrations (~10^5, 10^6, 10^7, and 10^8 CFU/mL) exported from the smartphone-based artificial intelligence cloud ($n = 3$ independent experiments). (D) mHealth system and commercial kit detection β-lactamase levels in *S. aureus* and MRSA ZJU, *E. coli* and *E. cloacae*, *K. pneumoniae*, and *K. pneumoniae* PKU (~10^5, 10^6, 10^7, 10^8 CFU/mL) in serum (pH 7.4), (E) sewage (pH 8.1) and (F) saliva (pH 6.8) samples at 25°C and 37°C ($n = 3$ independent experiments).

S. aureus (MRSA) groups (USA300 and ZJU clinical strain), extended-spectrum β-lactamase (ESBL) *E. coli*, *E. cloacae*, and *K. pneumoniae* (XJTU and PKU clinical strains) exceeded 1.1 and were significantly higher than those of the former. This result indicates that the mHealth system could successfully distinguish between the negative/positive strains of β-lactam drug-resistant bacteria (Figure 5B). Next, we exported the data on β-lactamase levels of these bacteria from the smartphone-based AI cloud (Figure 5C). To verify the accuracy of the mHealth system, we co-incubated the commercial kit (nitrocefin) with these strains and quantified β-lactamase levels using a UV spectrophotometer. The testing results based on the mHealth system showed a strong correspondence with the commercial kit (Supporting Information: Figure S9A). Next, we tested the minimum inhibitory concentration (MIC) of cephalothin required to inhibit the bacteria to determine whether these bacteria are resistant to antibiotics. The β-lactamase produced by these strains could considerably decrease the effectiveness of antibiotics. For the multidrug-resistant groups, the trend of the Rel. MIC values obtained were consistent with the results of the mHealth system (Supporting Information: Figure S9B). By comparing these methods, the test results can be mutually verified. However, considering the experimental procedures and operations, the commercial kit and the MIC method require the use of professional instruments and equipment to process the samples. At the same time, the sample processing and incubation time can be as long as several hours or more, which is considered cumbersome and time-consuming. In the mHealth system, it only takes a few minutes to identify drug-resistant bacteria and quantify β-lactamase levels in a simple way without trained operators.

To further validate its POCT capacity, the mHealth system detection of β-lactamase levels in various types of complex samples was evaluated. *S. aureus* is the most common pathogen in wound suppurative infections, *E. cloacae* is often detected in fecal water and soil, and *K. pneumoniae* exists in respiratory and intestinal tracts. Therefore, we selected three complex sample types: serum, sewage, and saliva. To verify the POCT performance, bacteria were added to serum, sewage, and saliva in the mHealth system. Different concentrations of drug-resistant bacteria were present. Based on the mHealth system, with the increase in the bacteria concentration, the β-lactamase level increased significantly. Meanwhile, the results of testing using the commercial kit closely correspond to our mHealth system (Figure 5D–F). This suggests that the performance of the mHealth system endowed the β-lactamase test with satisfactory accuracy and selectivity in POCT.

3.6 | mHealth system detection of β-lactamase in an animal infection model

Clinical practice is a critical part of POCT. To demonstrate the potential clinical significance of the mHealth system, we constructed an infection model of peritonitis and skin wound in mice. Then, the mHealth system was used to detect the level of β-lactamase secreted in the ascites and wound exudates of mice at different time points, and the results were also confirmed using the commercial kit. The bacteria concentration in ascites and exudates was determined by agar plate culture (Figure 6A).

First, the peritonitis model was created by injecting *E. coli* and ESBL *E. coli* into the abdomen of mice. When the inoculation concentration of ESBL *E. coli* was ~10^7 CFU/mL, the level of β-lactamase secreted and the bacteria number in the ascites significantly increased over time (0–24 h). However, when the inoculation concentration was ~10^5 CFU/mL, the β-lactamase level and the bacteria number in ascites slightly increased after 3 h, and then decreased to the horizontal level. This phenomenon may be attributed to the fact that the immune system of mice can kill the invading bacteria and prevent the development of infection.[40,41] When the inoculation concentration with sensitive-strain *E. coli* was ~10^5 and 10^7 CFU/mL, the bacteria number in ascites fluctuated over time, but the β-lactamase level was hardly detected (Figure 6B,C,F,G). The representation of the peritonitis model and organ damage level is shown in Supporting Information: Figure S10A.

Additionally, a skin wound infection model was created on the back of mice by inoculation of *S. aureus* and MRSA ZJU into full-thickness skin wounds. When the inoculation concentration of bacteria was ~10^7 CFU/mL, the bacteria number in the exudate increased with time (0–48 h), and the β-lactamase level infected with MRSA ZJU increased significantly but could not be detected in sensitive-strain *S. aureus*-infected wounds. When the inoculation concentration was ~10^5 CFU/mL, the bacteria number in the exudate decreased with time and β-lactamase was not detectable both in MRSA ZJU and in *S. aureus* (Figure 6D,E,H,I). This proved once again that the infection may not develop when the bacteria concentration is below ~10^5 CFU/mL. The representation of skin wounds and the exudate from wounds is shown in Supporting Information: Figure S10B. Meanwhile, all the above results of the mHealth system for detecting the β-lactamase levels in infected mice were further confirmed using the commercial kits (Supporting Information: Figure S11). These results suggest that the mHealth system has reliable clinical application value.
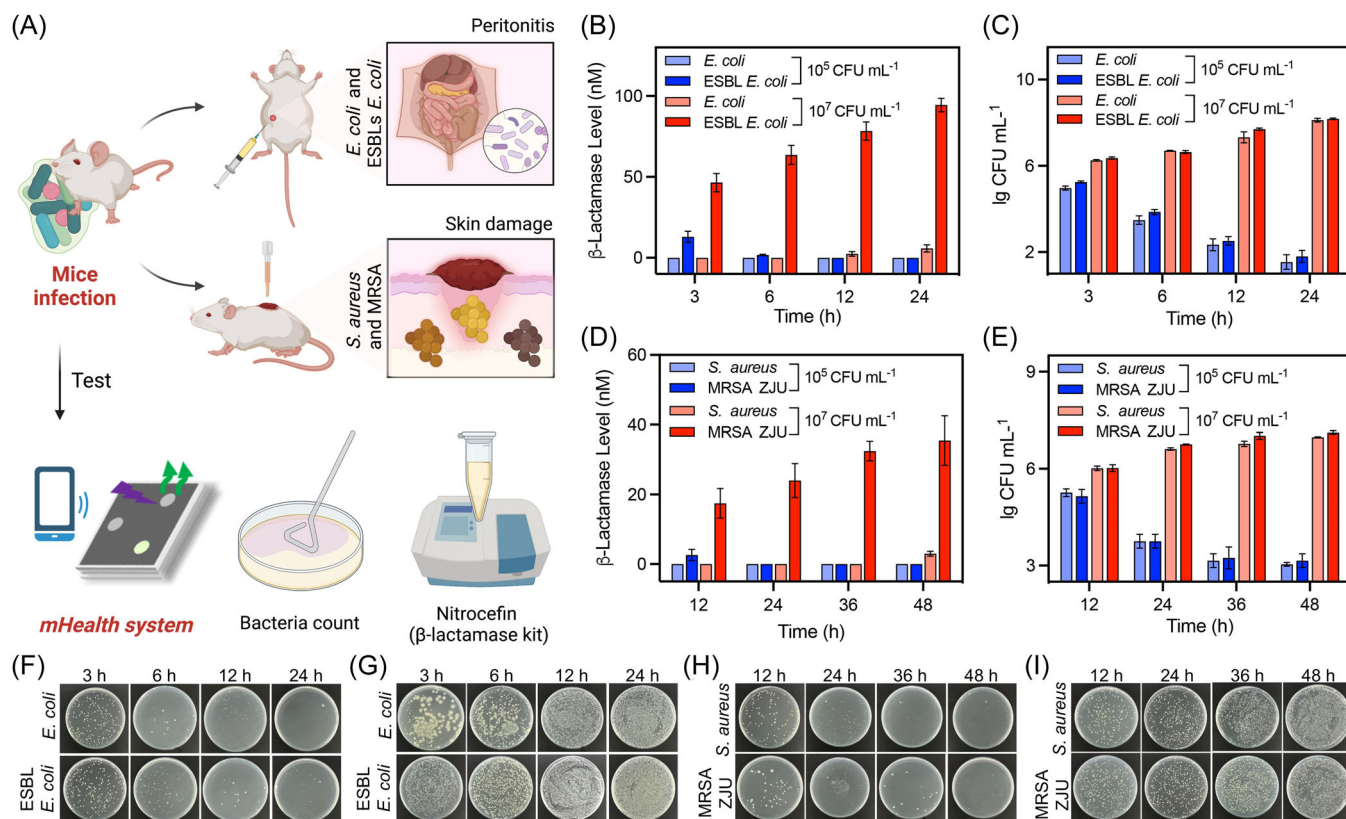
FIGURE 6 Determination of β-lactamase levels and bacteria in a mice infection model. (A) Schematic of mice peritonitis and skin wound infection model construction and determined by the mHealth system, the commercial kit, and agar plate culture. (B) mHealth system detection of β-lactamase levels in peritonitis infected with *Escherichia coli* (*E. coli*) and extended-spectrum β-lactamase (ESBL) *E. coli* (~10^5 and 10^7 CFU/mL) ($n = 3$ independent experiments). (C) In agar plate culture, the number of *E. coli* and ESBL *E. coli* is counted from ascites ($n = 3$ independent experiments). (D) mHealth system detection of β-lactamase levels in skin wound infected with *Staphylococcus aureus* (*S. aureus*) and multidrug-resistant *S. aureus* (MRSA) ZJU (~10^5 and 10^7 CFU/mL) ($n = 3$ independent experiments). (E) In agar plate culture, the number of *S. aureus* and MRSA ZJU is counted from exudate ($n = 3$ independent experiments). (F) Bacteria density of ascites from mice infected with *E. coli*. (G) ESBL *E. coli* [~10^5 and 10^7 CFU/mL] cultured by an agar plate. (H) Bacteria density of exudate from mice infected with *S. aureus* and (I) MRSA ZJU [~10^5 and 10^7 CFU/mL] cultured by an agar plate.

4 | CONCLUSION

In summary, we successfully fabricated an ultrafast response broad-spectrum fluorogenic probe (B1) that could rapidly respond to β-lactamase within 20 s, and established the mHealth system based on 3D B1-μPADs and a smartphone-based AI cloud. The developed mHealth system could diminish the influences of environmental temperature and pH, allowing the rapid and accurate detection of β-lactamase levels. Furthermore, the mHealth system has been evaluated in mice infection models, demonstrating that it can selectively and accurately identify drug-resistant bacteria and quantify the β-lactamase levels in complex biophysical environments. The system has potential clinical significance and excellent POCT ability with cost-effectiveness and convenience that make it affordable and accessible in most places, even in remote areas. We anticipate that this work will inspire new designs of ultrafast response fluorogenic probes and expedite the advancement of the "Chemical⁺ AI" analytical models of biomarker tracking that aim to combat AMR.

CONFLICTS OF INTEREST STATEMENT

The authors declare no conflicts of interest.

DATA AVAILABILITY STATEMENT

The data that support the findings of this study are available in the supplementary material of this article.

ETHICS STATEMENT

All the animal experiments in this study were conducted in accordance with the guidelines of the Administration of Laboratory Animals of China (2017 revision) and approved by the Animal Ethical Committee of Northwestern Polytechnical University (202201034).

ORCID

Lin Li http://orcid.org/0000-0003-0426-6546

REFERENCES

1. Blaser MJ. Antibiotic use and its consequences for the normal microbiome. *Science*. 2016;352(6285):544-545.
2. Laxminarayan R, Sridhar D, Blaser M, Wang M, Woolhouse M. Achieving global targets for antimicrobial resistance. *Science*. 2016;353(6302):874-875.
3. Sciarretta K, Røttingen JA, Opalska A, Van Hengel AJ, Larsen J. Economic incentives for antibacterial drug development: literature review and considerations from the transatlantic task force on antimicrobial resistance. *Clin Infect Dis*. 2016;63(11):1470-1474.
4. Durand-Reville TF, Miller AA, O'Donnell JP, et al. Rational design of a new antibiotic class for drug-resistant infections. *Nature*. 2021;597(7878):698-702.
5. Babic M, Hujer A, Bonomo R. What's new in antibiotic resistance? Focus on beta-lactamases. *Drug Resist Updat*. 2006;9(3):142-156.
6. Gajdács M. The continuing threat of methicillin-resistant *Staphylococcus aureus*. *Antibiotics*. 2019;8(2):52.
7. Zhang Y, Wang Q, Yin Y, et al. Epidemiology of carbapenem-resistant *Enterobacteriaceae* infections: report from the China CRE network. *Antimicrob Agents Chemother*. 2018;62(2):e01882-17.
8. Hu FP, Guo Y, Zhu DM, et al. Resistance trends among clinical isolates in China reported from CHINET surveillance of bacterial resistance, 2005-2014. *Clin Microbiol Infect*. 2016;22(1):S9-S14.
9. Xie H, Mire J, Kong Y, et al. Rapid point-of-care detection of the tuberculosis pathogen using a BlaC-specific fluorogenic probe. *Nat Chem*. 2012;4(10):802-809.
10. Cheng Y, Xie J, Lee KH, et al. Rapid and specific labeling of single live *Mycobacterium tuberculosis* with a dual-targeting fluorogenic probe. *Sci Transl Med*. 2018;10(454): eaar4470.
11. Mehta R, Rivera DD, Reilley DJ, et al. Visualizing the dynamic metalation state of New Delhi Metallo-β-lactamase-1 in bacteria using a reversible fluorescent probe. *J Am Chem Soc*. 2021;143(22):8314-8323.
12. Ding Y, Li Z, Xu C, et al. Fluorogenic probes/inhibitors of β-lactamase and their applications in drug-resistant bacteria. *Angew Chem Int Ed*. 2021;60(1):24-40.

13. Shatalin K, Nuthanakanti A, Kaushik A, et al. Inhibitors of bacterial H_2S biogenesis targeting antibiotic resistance and tolerance. *Science*. 2021;372(6547):1169-1175.
14. Nordmann P, Gniadkowski M, Giske CG, Poirel L, Woodford N, Miriagou V. Identification and screening of carbapenemase-producing *Enterobacteriaceae*. *Clin Microbiol Infect*. 2012;18(5):432-438.
15. Bernabeu S, Poirel L, Nordmann P. Spectrophotometry-based detection of carbapenemase producers among *Enterobacteriaceae*. *Diagn Microbiol Infect Dis*. 2012;74(1):88-90.
16. Cohen Stuart J, Leverstein-Van Hall MA. Guideline for phenotypic screening and confirmation of carbapenemases in *Enterobacteriaceae*. *Int J Antimicrob Agents*. 2010;36(3):205-210.
17. Savli H, Karadenizli A, Kolayli F, Gundes S, Ozbek U, Vahaboglu H. Expression stability of six housekeeping genes: a proposal for resistance gene quantification studies of *Pseudomonas aeruginosa* by real-time quantitative RT-PCR. *J Med Microbiol*. 2003;52(5):403-408.
18. Huang Y, Chen W, Chung J, Yin J, Yoon J. Recent progress in fluorescent probes for bacteria. *Chem Soc Rev*. 2021;50(13): 7725-7744.
19. Gao W, Xing B, Tsien RY, Rao J. Novel fluorogenic substrates for imaging β-lactamase gene expression. *J Am Chem Soc*. 2003;125(37):11146-11147.
20. Yao H, So M, Rao J. A bioluminogenic substrate for in vivo imaging of β-lactamase activity. *Angew Chem Int Ed*. 2007;46(37):7031-7034.
21. Chen Y, Xianyu Y, Wu J, Zheng W, Rao J, Jiang X. Point-of-care detection of β-lactamase in milk with a universal fluorogenic probe. *Anal Chem*. 2016;88(11):5605-5609.
22. Mao W, Xia L, Wang Y, Xie H. A self-immobilizing and fluorogenic probe for β-lactamase detection. *Chem Asian J*. 2016;11(24):3493-3497.
23. Li L, Li Z, Shi W, Li X, Ma H. Sensitive and selective near-infrared fluorescent off-on probe and its application to imaging different levels of β-lactamase in *Staphylococcus aureus*. *Anal Chem*. 2014;86(12):6115-6120.
24. Luo Z, Lv T, Zhu K, et al. Paper-based ratiometric fluorescence analytical devices towards point-of-care testing of human serum albumin. *Angew Chem Int Ed*. 2020;59(8):3131-3136.
25. Chu S, Wang H, Ling X, Yu S, Yang L, Jiang C. A portable smartphone platform using a ratiometric fluorescent paper strip for visual quantitative sensing. *ACS Appl Mater Interfaces*. 2020;12(11):12962-12971.
26. Boehle KE, Gilliand J, Wheeldon CR, et al. Utilizing paper-based devices for antimicrobial-resistant bacteria detection. *Angew Chem Int Ed*. 2017;56(24):6886-6890.
27. Arumugam S, Colburn DAM, Sia SK. Biosensors for personal mobile health: a system architecture perspective. *Adv Mater Technol*. 2020;5(3):1900720.
28. Tu J, Torrente-Rodríguez RM, Wang M, Gao W. The era of digital health: a review of portable and wearable affinity biosensors. *Adv Funct Mater*. 2020;30(29):1906713.
29. Liu J, Geng Z, Fan Z, Liu J, Chen H. Point-of-care testing based on smartphone: the current state-of-the-art (2017-2018). *Biosens Bioelectron*. 2019;132:17-37.
30. Li W, Wang M, Mille LS, et al. A smartphone-enabled portable digital light processing 3D printer. *Adv Mater*. 2021;33(35): 2102153.

31. Fang H, Zhang H, Li L, et al. Rational design of a two-photon fluorogenic probe for visualizing monoamine oxidase A activity in human glioma tissues. *Angew Chem Int Ed*. 2020;59(19):7536-7541.

32. Trott O, Olson AJ. AutoDock Vina: improving the speed and accuracy of docking with a new scoring function, efficient optimization, and multithreading. *J Comput Chem*. 2010;31(2):455-461.

33. Wu M, Suo F, Zhou J, et al. Paper-based fluorogenic device for detection of copper ions in a biological system. *ACS Appl Bio Mater*. 2018;1(5):1523-1529.

34. Wiegand I, Hilpert K, Hancock REW. Agar and broth dilution methods to determine the minimal inhibitory concentration (MIC) of antimicrobial substances. *Nat Protoc*. 2008;3(2):163-175.

35. Xie J, Zhou M, Qian Y, et al. Addressing MRSA infection and antibacterial resistance with peptoid polymers. *Nat Commun*. 2021;12(1):5898.

36. Stjerndahl M, Lundberg D, Chauhan V, Bordes R, Holmberg K. Cleavable surfactants: a comparison between ester, amide, and carbonate as the weak bond. *J Surfactants Deterg*. 2019;22(5):1139-1145.

37. Xue Y, Bai H, Peng B, et al. Stimulus-cleavable chemistry in the field of controlled drug delivery. *Chem Soc Rev*. 2021;50(8):4872-4931.

38. Roose BW, Zemerov SD, Wang Y, Kasimova MA, Carnevale V, Dmochowski IJ. A structural basis for ^{129}Xe hyper-CEST signal in TEM-1 β-lactamase. *Chemphyschem*. 2019;20(2):260-267.

39. Doughty MJ. pH dependent spectral properties of sodium fluorescein ophthalmic solutions revisited. *Ophthalmic Physiol Opt*. 2010;30(2):167-174.

40. Church D, Elsayed S, Reid O, Winston B, Lindsay R. Burn wound infections. *Clin Microbiol Rev*. 2006;19(2):403-434.

41. Zhang J, Jia Q, Yue Z, et al. An electroluminodynamic flexible device for highly efficient eradication of drug-resistant bacteria. *Adv Mater*. 2022;34(17):2200334.

SUPPORTING INFORMATION

Additional supporting information can be found online in the Supporting Information section at the end of this article.

How to cite this article: Ding Y, Chen J, Wu Q, et al. Artificial intelligence-assisted point-of-care testing system for ultrafast and quantitative detection of drug-resistant bacteria. *SmartMat*. 2023;e1214. doi:10.1002/smm2.1214